Organic & Biomolecular Chemistry

A Modular Approach for Organizing Dimeric Coiled Coils on Peptoid Oligomer Scaffolds

Journal:	*Organic & Biomolecular Chemistry*
Manuscript ID	OB-ART-03-2020-000453
Article Type:	Paper
Date Submitted by the Author:	21-Dec-2019
Complete List of Authors:	Kirshenbaum, Kent; New York University, Chemistry; New York University Jiang, Linhai; New York University, Chemistry

ARTICLE

A Modular Approach for Organizing Dimeric Coiled Coils on Peptoid Oligomer Scaffolds†

Received 00th January 20xx,
Accepted 00th January 20xx

DOI: 10.1039/x0xx00000x

Linhai Jiang and Kent Kirshenbaum*

We report a general approach to promote the folding of synthetic oligopeptides capable of forming homodimeric coiled coil assemblies. By pre-organizing the peptides on macrocyclic oligomer scaffolds, the stability of the coiled coils is enhanced with an observed increase in the melting temperature of 30 ℃ to 40 ℃. Molecular dynamics simulations substantiate the hypothesis that the enhanced stability is established by constraining motion at the peptide termini and by pre-organizing intramolecular helix-helix contacts. We demonstrate the modularity of this approach by using a family of peptoid scaffolds to promote the folding of a dimeric coiled coil. Importantly, this strategy for templating coiled coils allows preservation of native amino acid sequences. Comparing a macrocyclic peptoid scaffold to its linear counterparts indicates that both types of assemblies are effective for organizing stable coiled coils. These results will guide future designs of coiled coil peptides for biomedical applications and as building blocks for more complex supramolecular assemblies.

Introduction

Coiled coils are important and ubiquitous protein structural motifs, and are involved in many critical biological events, such as gene expression, muscle contraction, cellular transport and signaling.[1-4] Coiled coils are formed by two or more right-handed α-helices that associate to form left-handed multi-stranded supercoils.[5-8] Dimeric coiled coils are of particular interest due to their structural simplicity and designability. De novo designed dimeric coiled coils have been extensively utilized as building blocks for constructing self-assembled nanometer-scale architectures and as potential therapeutics for targeting protein-protein interactions.[7, 9-18] Enhancing the stability of coiled coils can expand their capability to address functional goals.[19-21]

The amino acid sequence of coiled coil peptides typically features a heptad repeat pattern (***abcdefg***), based on the different contributions of each residue within the repeat unit to characteristic non-covalent interactions.[7] The formation of a dimeric coiled coil is primarily driven by the hydrophobic contacts among residues at ***a*** and ***d*** positions in the heptad pattern. Inter- and intra-helical electrostatic interactions between oppositely charged residues at ***g*** and ***e*** positions make further contributions to coiled coil stability. Several strategies have been reported to improve and/or tune the stabilities of synthetic dimeric coiled coils, such as elongating the peptide chains,[22] substitution of leucine at ***d*** positions by 5,5,5-trifluoroleucine,[23] installing inter-helical disulphide or thioether linkages,[24-28] optimizing the inter- and intra-helical electrostatic interactions,[29-30] replacing inter-helical non-covalent salt bridges by covalent linkages[31-32] and incorporation of histidine-metal coordination sites within the coiled coils[33].

The aforementioned methods are all capable of elevating the thermal stability of dimeric coiled coils, but generally require altering the original amino acid sequences, which may influence the native functions associated with the coiled coils. Alternative methods that can enhance coiled coil thermal stability while preserving the original amino acid sequence would be desirable for a wider range of applications. We considered how individual peptide chains comprising dimeric coiled coils may disassociate and unfold upon thermal denaturation. Because unfolding is associated with helix fraying at peptide termini, we envisioned that confining peptides in proximity while constraining the termini might promote coiled coil stability without necessitating modifications to the amino acid sequences. This approach is similar to the Template Assembled Synthetic Proteins (TASP) strategy,[34-42] in which the termini of multiple helical peptides are anchored to organic macrocyclic scaffolds, such as porphyrins, Kemp's triacid, or cyclotribenzylene. The TASP strategy primarily focuses on inducing and/or increasing the folding ability of trimeric and tetrameric coiled coils. Surprisingly, few efforts have been made to investigate the effect on dimeric coiled coils.[36] The rigidity and symmetry of the template scaffolds have proven to be advantageous for implementing TASP strategies effectively.[36-37] In addition to the TASP strategy, assembly of three-helix bundles has also been

Chemistry Department, New York University, New York, NY 10003, United States. E-mail: kk54@nyu.edu

† Electronic Supplementary Information (ESI) available: Experimental details, simulation protocols and supplementary data. See DOI: 10.1039/x0xx00000x

directed through metal-coordination at N-terminal positions incorporating 2,2'-bipyridine units.[43-44]

We considered whether peptoids, N-substituted glycine oligomers, could also be used as scaffolds to pre-organize two peptide chains in proximity and to enhance the stability of dimeric coiled coils. Peptoids are attractive scaffolds for multivalent display.[45-49] In comparison to most scaffolds previously used for TASP strategies, peptoids are highly modular molecules that can be readily synthesized using solid phase synthesis techniques to include a remarkable diversity of side chain functional groups at precise positions along the oligomer sequence.[50-51] Similar to peptides, the backbone rigidity of peptoids can be controlled by incorporation of torsionally constrained residues, such as proline derivatives,[52, ‡] and by head-to-tail macrocyclization[53-54]. In this work, we employed a combination of experimental and computational approaches to explore how peptoids can serve as scaffolds for dimeric coiled coils and to demonstrate how their modular synthesis can readily provide a family of effective scaffolds for de novo design of protein mimetics.

Results and discussion

We initiated an effort to design a parallel coiled coil dimer scaffolded onto an oligomeric macrocycle. We selected to incorporate a peptide named **GCNshSN**, used by the Jerala group to construct a protein-origami cage.[14, 55] Based on the amino acid sequence, **GCNshSN** exclusively forms parallel coiled coil homodimers (Scheme 1A). The inclusion of asparagine (Asn) at the ***a*** position of the third heptad pattern confers the specific formation of a parallel and in-register dimer due to the self-complementary hydrogen bonding between side-chain amide groups of Asn pairs at the helix-helix interface.[56]

We contemplated the option of tethering either the N- or C-termini of the peptide strands to the macrocyclic scaffold. We reasoned that conjugation of the more flexible terminus would lead to greater stability of the folded coiled coil. We conducted molecular dynamics (MD) simulation studies to compare the flexibility of the C-termini and N-termini of the coiled-coil forming peptides. The simulations were conducted at 278 K using the AMBER Force Field ff14SBonlysc[57-58] and the GB-Neck2[59] implicit solvent model. The initial conformation of the **GCNshSN** coiled coil dimer was modeled using the crystal structure of the parent peptide (pdb code: 2zta).[55] The native coiled coil tertiary structure was well maintained by the **GCNshSN** peptides over the course of 1 μs MD simulations. The α-helical secondary structure content fluctuated around 80% (Figure 1A left) and superimposition of the simulated averaged conformation to the crystal structure produced a Cα root mean square deviation (RMSD) value of 0.88 Å (Figure 1B). In addition, we found that the N-termini of coiled coils formed by individual peptides were more flexible than the C-termini (Figure 1D left). Thus, we concluded that it would be preferable to stabilize the coiled coil by conjugating the two individual peptide chains to the macrocyclic peptoid scaffold through their N-termini.

A six-residue peptoid macrocycle (Scheme 1B), denoted as **Meta596**, incorporating three proline residues and three N-substituted glycine residues (one N-methoxyethyl peptoid residue and two N-propargyl peptoid residues) at alternating positions, was used as a divalent scaffold to pre-organize the

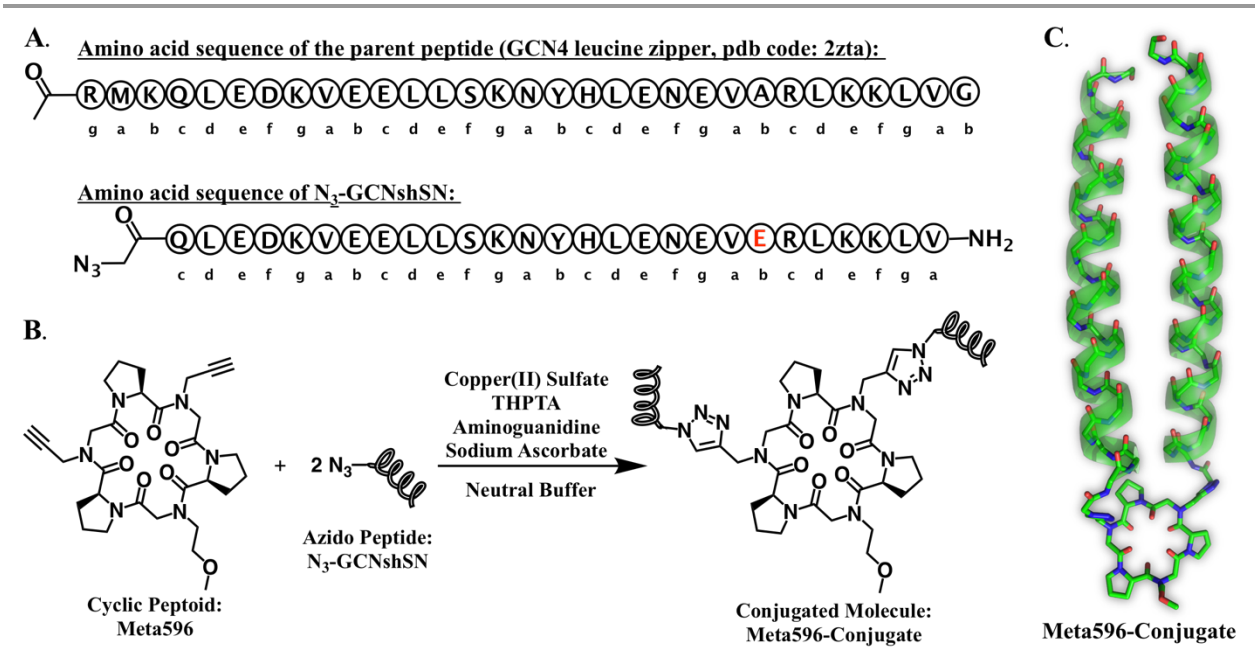

Scheme 1. (A) Amino acid sequence of **N_3-GCNshSN** and its parent peptide, the GCN4 leucine zipper. Each amino acid residue is represented by the circled one letter code. The chemical structures of N- and C-terminal capping groups are shown explicitly. A single site mutation is highlighted in red.[14, 55] The heptad pattern is indicated by lower case letters below each residue. (B) Synthetic route to prepare peptoid-peptide conjugates via copper(I)-catalyzed azide-alkyne cycloaddition click chemistry, as exemplified for the synthesis of **Meta596-Conjugate**. (C) Cartoon representation of the **Meta596-Conjugate** product as rendered by PyMOL (Schrödinger, LLC).

two peptide chains. This peptoid macrocyclic oligomer sequence was selected because a high-resolution crystal structure of an analog, in which the two propargyl side chains are replaced by methoxyethyl sidechains, has been previously reported.[60] This crystal structure reveals a roughly planar macrocycle in which the three methoxyethyl side chains are extended laterally, enabling efficient conjugation at these sites (Figure S6). Our macrocycle design featured replacement of two of the methoxyethyl side chains with N-propargyl side chains groups to enable subsequent conjugation of **N_3-GCNshSN** peptides bearing N-terminal azido groups through copper(I)-catalyzed azide-alkyne cycloaddition (CuAAC) reactions to form the **Meta596-Conjugate** (Scheme 1B and 1C). We also conducted MD simulations of the **Meta596-Conjugate** using the GAFF2[61] forcefield to model the peptoid component. As expected, this simulation provided a stable coiled coil intramolecular assembly at 278 K over the course of 1 μs (Figure 1A right and 1C). The simulation revealed that the N-terminal flexibility of the **GCNshSN** peptides was significantly diminished by the formation of the conjugated species to pre-organize the coiled coils (Figure 1D right).

Chemical synthesis was initiated with the solid phase assembly of the **GCNshSN** peptide. This was conducted on Rink Amide MBHA resin using standard Fmoc chemistry. Following completion of the peptide sequence, 2-azidoacetic acid was used to cap the peptide and provide the desired reactive group at the N-terminus (Scheme 1A). The peptides were purified by HPLC to 95% purity. Next, the peptoid macrocycle scaffold was assembled. The linear oligomer sequence was synthesized on 2-chlorotrityl chloride resin using a combination of peptoid "submonomer" protocols[50] (N-methoxyethyl glycine and N-propargyl glycine positions) and Fmoc synthesis protocols[12] (proline positions). The linear oligomer was subjected to head-to-tail macrocyclization by formation of the intramolecular amide bond in the presence of PyBOP as an activating agent to form the hexamer macrocycle product **Meta596**.[62] The **N_3-GCNshSN** and **Meta596** species were then conjugated through triazole linkages formed via a CuAAC click chemistry protocol modified from a reported method (Scheme 1B).[63] The conjugation reaction went to completion after 24hrs with a yield >90%.

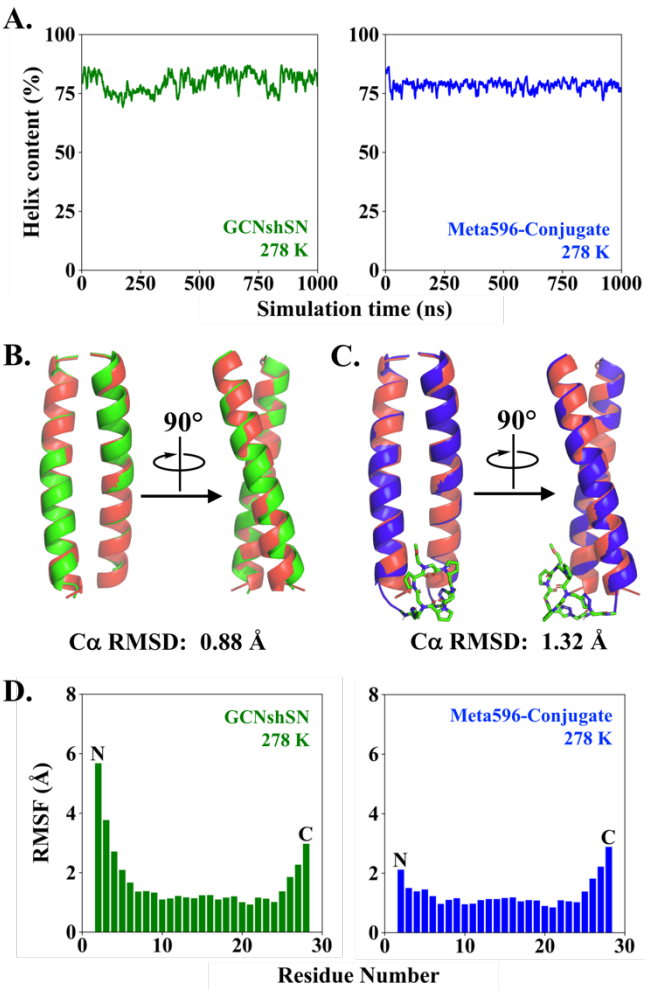

Figure 1. Results of a representative 1 μs Molecular Dynamics simulation conducted at 278 K. (A) α-Helical content of the dimeric coiled coil adopted by **GCNshSN** peptides and **Meta596-Conjugate** over the course of the simulation. Comparison of the coiled coil crystal structure (red in B and C) and averaged conformations simulated by molecular mechanics using the unconjugated **GCNshSN** peptide (green in B) and **Meta596-Conjugate** (blue in C, peptoid component is shown in sticks), respectively. (D) Residue-based root mean square fluctuation (RMSF) analysis of coiled coils formed by **GCNshSN** peptide and **Meta596-Conjugate**. N- and C-termini are indicated within the bar plots. RMSF values are averaged from two chains for fluctuation of peptide backbone atoms only: C, N and Cα. See Supporting Information for the analysis of other results.

The secondary structures of **Meta596-Conjugate** and the unconjugated **N_3-GCNshSN** peptides were experimentally assessed by Circular Dichroism (CD) spectroscopy. Minima in the CD spectra were observed at both 208 nm and 222 nm (Figure 2A and 2B), indicative of α-helical conformation for both molecules at 25 °C.[64-65] The CD signal near 208 nm is associated with amide π→π* transitions that are polarized parallel to the helical axis. The strength of this signal is correlated with increased helix-helix contacts.[66] The second minimum around 222 nm is caused by amide n→π* transitions and is not strongly influenced by contacts at the helix-helix interface. Thus, the ratio of the MRE value at 222 nm to that at 208 nm ($\theta_{222}/\theta_{208}$) has been generally used to monitor the presence of coiled coils formed by α-helices.[67-68] Typically, a ratio in the range of 0.9 indicates the presence of both individual α-helical secondary structure elements and helices within the coiled coils. In contrast, $\theta_{222}/\theta_{208}$ values close to 1.0 suggest a negligible presence of single-chain helices and the predominance of coiled-coil species. We observed a $\theta_{222}/\theta_{208}$ ratio of 0.84 for the unconjugated **N_3-GCNshSN** peptides at 25 °C (Figure 2A), while this value was 0.96 for the **Meta596-Conjugate** (Figure 2B). The CD studies thus indicate enhanced helix-helix contacts associated with the formation of stable coiled coils for the **Meta596-Conjugate**, relative to the unconjugated peptides.

By monitoring the temperature-dependent CD signal at 222 nm, thermal denaturation studies were carried out to investigate the effect of conjugation on coiled coil thermal stabilities. The midpoint of the unfolding transition, T_M, was used to characterize the thermal stability of the folded

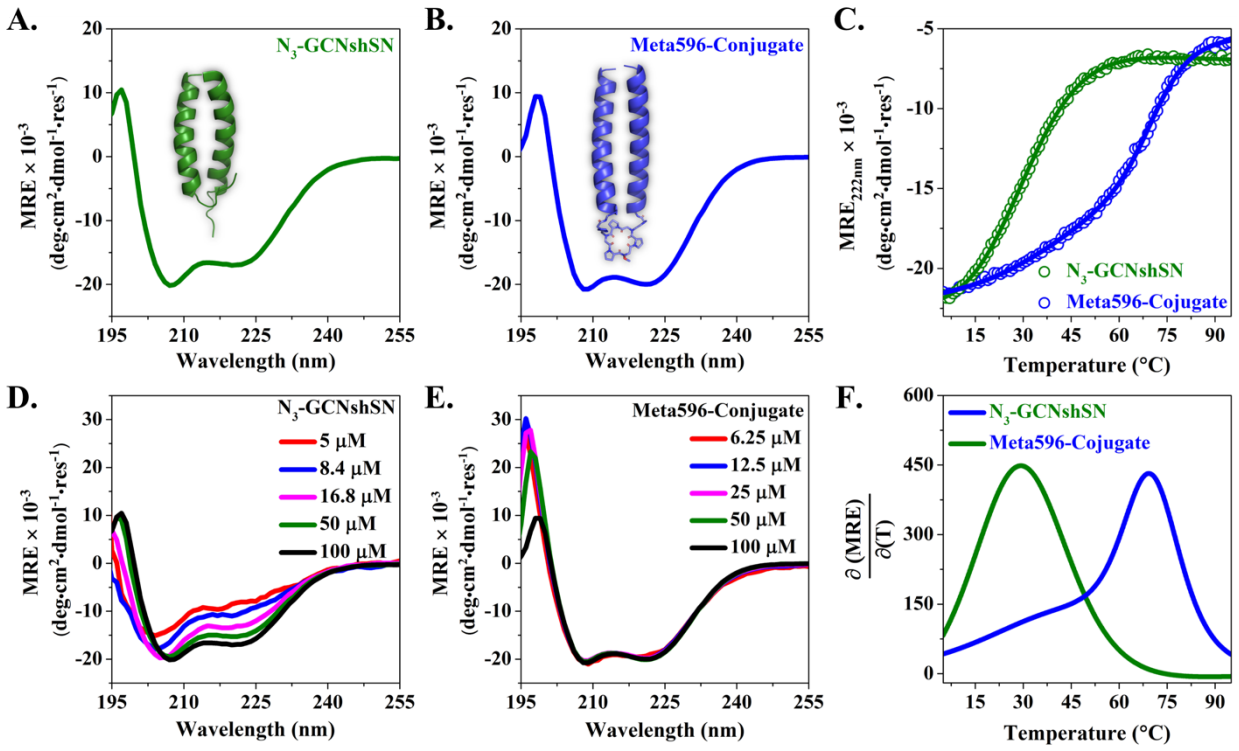

Figure 2. Circular Dichroism (CD) spectra of **N_3-GCNshSN** peptides (A) and **Meta596-Conjugate** (B). (C) Thermal denaturation profiles of **N_3-GCNshSN** peptides and **Meta596-Conjugate**. Circles: experimental data points; solid line: sigmoidal fittings using BiDoseResp function implemented in OriginPro 8.5.1 (OriginLab Corporation). Concentrations (with respect to peptide chains): 100 μM. CD spectra of **N_3-GCNshSN** peptides (D) and **Meta596-Conjugate** (E) at varying concentrations. (F) First order derivatives of the sigmoidal fittings in (C), from which the melting temperature, T_M, was estimated.[54] Solvent: 10 mM sodium phosphate-150 mM sodium chloride buffer, pH 7.5. MRE: molar residue ellipticity. The CD signal contributed by the peptoid macrocycle has been subtracted. The CD spectra shown in (A), (B), (D) and (E) were measured at 25 °C.

peptides.[65] As shown in Figure 2C, cooperative unfolding transitions were observed for both individual peptides and conjugated species. Upon heating, the **Meta596-Conjugate** unfolded at a significantly elevated temperature compared to the individual **N_3-GCNshSN** peptides. The T_M of individual peptides was measured ~29 °C. In contrast, the **Meta596-Conjugate** exhibited a much higher T_M of ~69 °C. Thus, an increase of the T_M by 40 °C was obtained by constraining the N-termini of two peptide chains in proximity upon the cyclic peptoid scaffold.

The particular **GCNshSN** peptide sequences used in this study are known to exclusively form parallel homodimeric coiled coils.[14, 55] The **Meta596-Conjugate** was obtained through the formation of triazole linkages upon cycloaddition between the N-terminal azido groups of two peptide chains and the two sidechain alkyne groups displayed on the cyclic peptoid. Thus, the **Meta596-Conjugate** should also pre-organize the two conjugated peptide chains on the macrocyclic scaffold in a parallel alignment. We therefore anticipated that intramolecular helix-helix dimerization would be more favorable than intermolecular helix-helix dimerization for the **Meta596-Conjugate**.

To explore the organization of the coiled-coils formed by the **Meta596-Conjugate**, CD spectra were measured for samples at varying concentrations (Figure 2D and 2E). The CD spectra of the **Meta596-Conjugate** were nearly identical over the examined concentration range (from 5 μM to 100 μM at 25 °C). In contrast, for the unconjugated **N_3-GCNshSN** peptides, the content of α-helical secondary structure markedly diminished as the concentration was decreased. This concentration dependence is consistent with intermolecular helix-helix dimerization as the only pathway to form coiled coil structures for the individual **N_3-GCNshSN** peptides. The observed concentration independence of the helical conformation of the **Meta596-Conjugate** confirms that intermolecular association is negligible for this species, and that the coiled coils result predominantly from intramolecular helix-helix dimerization and parallel alignment as encoded in the amino acid sequence. Dynamic light scattering (DLS) analysis show that coiled coils formed by both unconjugated **N_3-GCNshSN** peptides and **Meta596-Conjugate** have hydrodynamic diameters ~2 nm, further confirming the absence of larger sized species that would be formed by **Meta596-Conjugate** through intermolecular associations (Figure S5).

Molecular dynamics simulations were performed to investigate the origins of the improved thermal stability of coiled coils formed by **Meta596-Conjugate**. The simulations were performed at 303 K, a temperature close to the experimental T_M of the individual peptides, but far below the T_M of the conjugate. The Rg (radius of gyration), backbone RMSD and helix content were used to monitor the deviation of the simulated structure from the fully folded conformation over the course of the simulations. Unrecoverable deviations

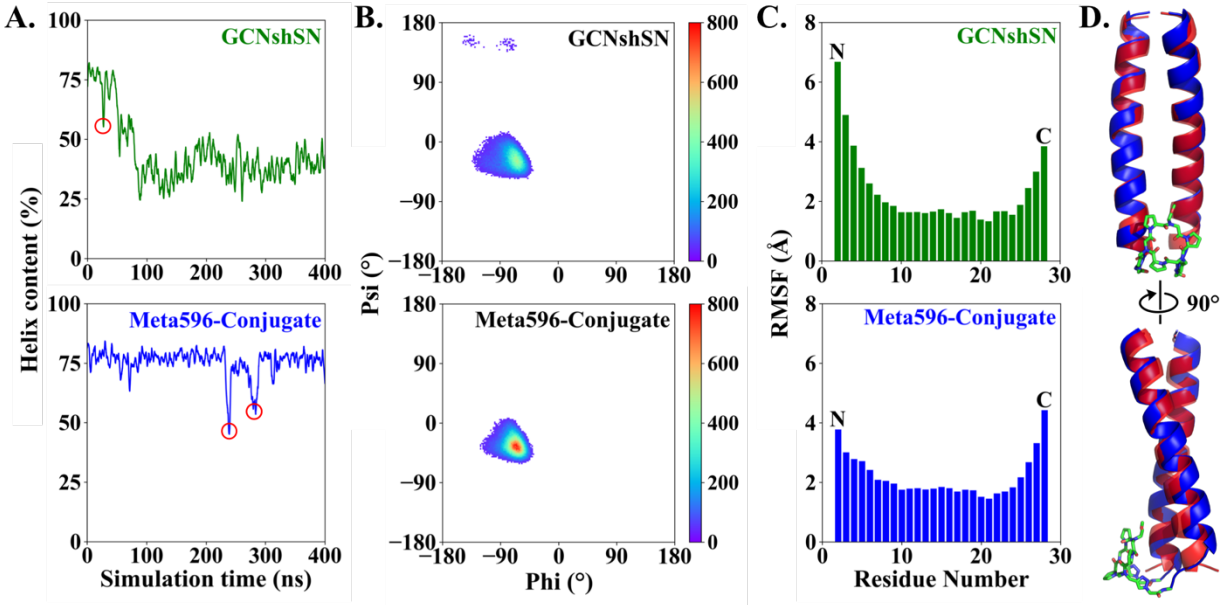

Figure 3. Results of 400 ns MD simulations at 303 K. (A) Helix content in the coiled coils formed by **GCNshSN** peptides (top) and **Meta596-Conjugate** (bottom). Red circles indicate unfolding-refolding equilibria. (B) Ramachandran maps of conformational space sampled by **GCNshSN** peptides and **Meta596-Conjugate** over the time course of the simulation. (C) Residue-based RMSF analysis of coiled coils formed by **GCNshSN** peptides within the folded region and **Meta596-Conjugate** over the time course of the simulation. RMSF values are averaged from two chains using atomic fluctuation of backbone atoms only: C, N and Cα. (D) Superimposition of the coiled coil crystal structure (red) and averaged conformation simulated by molecular mechanics using **Meta596-Conjugate** (blue) at 303 K. The peptoid component is shown in stick representation. See SI for analysis of other results and information from four other independent trajectories.

from the initial values were indicative of extensive long timescale unfolding in the simulation, while fluctuations with relatively large amplitudes indicated reversible unfolding-refolding equilibria. The individual peptides were extensively unfolded during the course of all five independent MD trajectories. For example, during one representative trajectory, the intermolecular coiled coil formed by individual peptides rapidly disassembled into two partially folded single-chain helices within the first 50 ns. The dissociation of two helical chains caused the helicity to decrease from ~78% to ~35%, with both Rg and RMSD deviating significantly from the initial values (Figure 3A top, Figure S11 and S13). The conformational space sampled by **GCNshSN** peptides fluctuated away from the ideal α-helix region (around $\varphi = -60°, \psi = -45°$) in the Ramachandran plot (Figure 3B, top). However, simulations for the **Meta596-Conjugate** consistently yielded stable coiled-coil forms with the backbone dihedral angles (φ, ψ) densely located in the ideal α-helix region in the Ramachandran map. Multiple reversible unfolding-refolding transitions were observed for **Meta596-Conjugate** over the course of MD simulations (Figure 3A bottom, S12, S14 and S16). For instance, in one trajectory (Figure 3A bottom), the coiled coil partially unfolded at 230 ns to a state with 30% less helix content. Due to the proximity of N-termini, the two peptide strands within the **Meta596-Conjugate** were able to quickly reassemble to the folded coiled coil structure within the following 25 ns. The Rg of each chain was maintained at ~13 Å with negligible deviation over the course of the simulation (Figure S14). Superimposition of the simulated averaged coiled coil conformation adopted by Meta596-Conjugate to the crystal structure produced a Cα RMSD value of 1.55 Å (Figure 3D). Some reversible unfolding-refolding transitions were also observed for the individual GCNshSN peptides prior to complete dissociation between the two peptide strands. However, only minor transient excursions from the fully folded conformation were tolerated without irreversible unfolding (Figure 3A top, S11, S13 and S15).

Based on their dramatically different thermal stabilities, the unconjugated **GCNshSN** peptides and **Meta596-Conjugate** exhibit distinct characteristics in the MD simulations at 303 K. In agreement with the experimental results, the coiled coil formed by the **Meta596-Conjugate** is much more thermostable than that formed by unconjugated **GCNshSN**

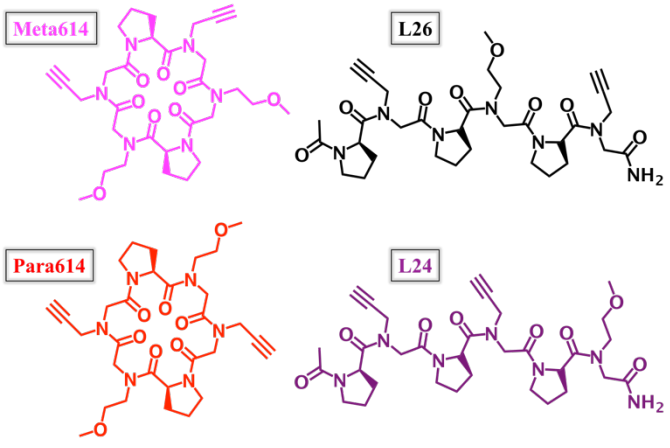

Scheme 2. Chemical structures of four additional peptoid scaffolds for pre-organizing dimeric coiled coils. **Meta614** and **Para614** cyclic peptoids are constitutional isomers, **L26** and **L24** are the linear counterparts of the **Meta596** cyclic peptoid.

peptides. RMSF analysis of the unconjugated **GCNshSN** peptides within the folded region shows that the N-termini are more flexible than C-termini (Figure 3C top and S19), suggesting that the unfolding of the coiled coil was initiated by the loss of critical helix-helix contacts at N-termini. In comparison, the N-terminal stabilities of the helical peptide components within the **Meta596-Conjugate** are comparable to the C-termini (Figure 3C bottom and S20). This is consistent with the maintenance of helix-helix contacts at the N-termini afforded by the covalent constraints. Overall, diminished flexibility at the N-termini and increased productive helix-helix collision frequencies may both play a role in the enhanced thermal stability of **Meta596-Conjugate** coiled-coil relative to the individual **GCNshSN** peptides.

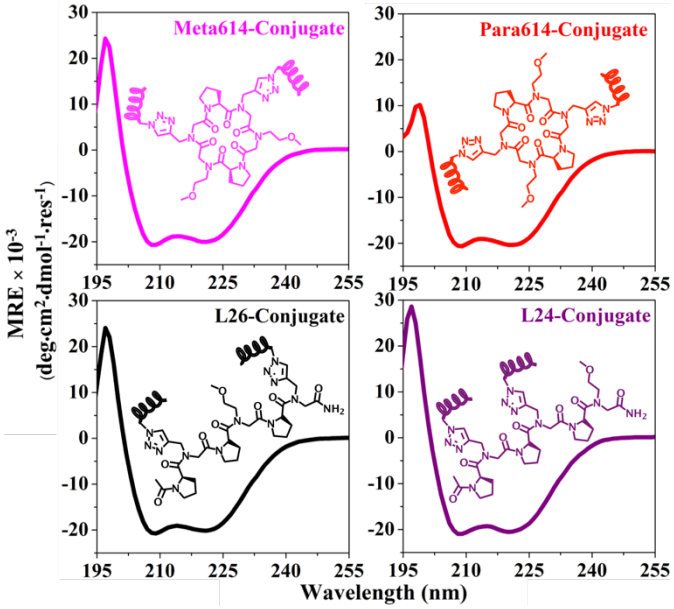

Figure 4. CD spectra of four dimeric coiled coils templated onto scaffold analogs: **Meta614-Conjugate** (upper left), **Para614-Conjugate** (upper right), **L26-Conjugate** (lower left) and **L24-Conjugate** (lower right). Chemical structure of each conjugated molecule is insetted to the corresponding CD spectrum. Helical elements indicate the **GCNshSN** peptide, as in Scheme 1. Concentration (with respect to peptide chains): 100 μM; solvent: 10 mM sodium phosphate-150 mM sodium chloride buffer, pH 7.5; temperature: 25 ℃. CD signals contributed by peptoid macrocycles have been subtracted.

In order to demonstrate the modularity of the peptoid oligomer templation strategy, four additional conjugated species were also synthesized and characterized by using four different peptoid scaffolds (Scheme 2). **Meta614-Conjugate** and **Para614-Conjugate** were synthesized using cyclic peptoid scaffolds that feature variations of the **Meta596** scaffold oligomer sequence. For the peptoid macrocycle components, both **Meta614-Conjugate** and **Para614-Conjugate** bear two proline residues at positions i and i+3. The two peptide strands were conjugated to the macrocyclic scaffolds through propargyl side chains located three residues apart for **Para614-Conjugate**, and two residues apart for **Meta614-Conjugate**. The other sidechain positions in the cyclic peptoids include methoxyethyl groups. In addition, two linear conjugates, **L26-Conjugate** and **L24-Conjugate**, were synthesized using two linear hexamer-analogs of the **Meta596** macrocyclic peptoid as the molecular scaffolds. In the **L26-conjugate**, the two peptide strands were conjugated to propargyl groups located four residues apart on the linear peptoid. For the **L24-conjugate**, the two peptide chains were conjugated at side chain positions two residues apart.

CD spectra characteristic of coiled coils ($\theta_{222}/\theta_{208}$ > 0.95) were observed for each of the conjugated molecules (Figure 4). The dimeric coiled coils formed by these conjugated molecules consistently displayed substantial enhancements in thermal stability relative to the individual peptides, with T_M values spanning from ~60 ℃ to ~70 ℃ (Figure 5). Indeed, the conjugated molecules established on linear peptoid scaffolds (**L26-Conjugate** and **L24-Conjugate**) enhanced the folding of coiled coils to a roughly similar extent as the macrocyclic counterpart (**Meta596-Conjugate**). The T_M value of **L24-Conjugate** is 2 ℃ higher than **Meta596-Conjugate** and the T_M of **L26-Conjugate** is 1 ℃ lower than **Meta596-Conjugate**. **Para614-Conjugate** enhanced the folding of coiled coil with a T_M 8 ℃ lower than **Meta596-Conjugate**, and **Meta614-Conjugate** promoted the coiled coil thermal stability with a T_M value only 2 ℃ lower than **Meta596-Conjugate**.

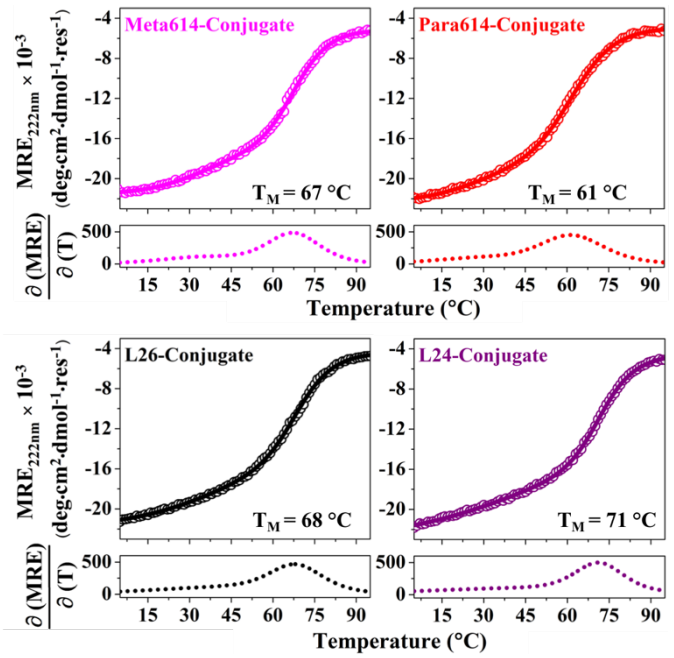

Figure 5. Thermal denaturation profiles of additional four dimeric coiled coils incorporation variations in the oligomeric templates, **Meta614-Conjugate** (upper left), **Para614-Conjugate** (upper right), **L26-Conjugate** (lower left) and **L24-Conjugate** (lower right). Concentration (with respect to peptide chains): 100 μM; solvent: 10 mM sodium phosphate-150 mM sodium chloride buffer, pH 7.5. CD signals contributed by peptoid macrocycles have been subtracted.

In the context of the macrocyclic constrained oligomer scaffolds, placement of the helices two residues apart may provide a slight improvement in pre-organizing the dimeric coiled coils (T_M = 67 ℃ versus T_M = 61 ℃ for placement three residues apart). For the linear oligomers, conformational rearrangements may allow these scaffolds to position the appended peptides optimally for coiled coil formation (T_M

values are approximately equivalent). The similar melting temperatures shown by **Meta596-Conjugate** (69 ℃) and its two linear counterparts, **L26-Conjugate** (68 ℃) and **L24-Conjugate** (71 ℃), indicate that macrocyclization of the peptoid oligomer scaffolds is not an essential feature in order to attain significant enhancement of thermal stabilities for templated coiled coils. This finding is not necessarily anticipated from previous studies utilizing the TASP strategy, in which four-helix bundles anchored by cyclic templates are more stable than those anchored by acyclic templates.[37] In addition, comparison of the **Meta596-Conjugate** and **Meta614-Conjugate** suggests that variations in scaffold composition can be readily tolerated. It is also possible to tune the coiled coil thermal stability by altering the relative positions of the conjugation sites on the peptoid scaffolds, as reflected by the differences in T_M between the **Meta614-Conjugate** and **Para614-Conjugate**. The coiled coil formation relied predominantly on intramolecular helix-helix dimerization for all the additional conjugated species, as evidenced by the concentration-independent CD spectra (Figure S4), along with hydrodynamic diameters in the range of 2 nm - 3 nm as measured by Dynamic Light Scattering (Figure S5).

Conclusions

In summary, we have promoted the folding of dimeric coiled coils by pre-organizing two helical peptide chains on designed peptoid oligomer scaffolds in a controlled fashion. Such pre-organization was achieved by conjugating the N-termini of two coiled-coil forming peptides to peptoid side chains using Cu(I)-catalyzed azide-alkyne cycloaddition reactions. Restricting the two N-termini in proximity enforces the formation of intramolecular coiled-coil assemblies. Macrocyclization of peptoid scaffolds was not required in order to significantly enhance the coiled coil thermal stabilities, whereas the relative sequence positions of two peptide chains appended to oligomeric scaffolds proved to be more important. Due to the built-in backbone rigidity and the conformational constraint, the macrocyclic peptoid scaffolds may be preferable for displaying multiple peptide chains that exclusively allow specific intermolecular associations in the construction of pre-determined nano/micro-sized supramolecular architectures. Molecular Dynamics simulations indicated that the enhanced thermal stabilities of the templated coiled-coils were established by diminishing conformational heterogeneity at the N-termini along with promoting helix-helix collision frequencies. The use of peptoid oligomers for templated self-assembly of peptide secondary structures will provide valuable constituents for design of more elaborate biomimetic architectures.[69-70] These results will expand the capabilities of coiled coils for nanoengineering and biomedical applications.

Conflicts of interest

There are no conflicts to declare.

Acknowledgements

Computer simulations were conducted with the assistance of NYU's IT High Performance Computing resources, services, and staff expertise. We acknowledge the contribution of James Eastwood for assistance with this manuscript. The Circular Dichroism Spectropolarimeter used in this work was acquired through the support of New York University. This work was supported by the National Science Foundation (Award CHE-1507946 to K.K.).

Notes and references

‡: Although proline is among the set of proteinogenic polypeptide monomers, because they are N-substituted α-amino acids, we refer to them in this report also as peptoid monomers.

1 P. Burkhard, J. Stetefeld and S. V. Strelkov, *Trends Cell Biol.,* 2001**, 11,** 82-88.
2 J. M. Mason and K. M. Arndt, *ChemBioChem,* 2004**, 5,** 170-176.
3 H. R. Marsden and A. Kros, *Angew. Chem. Int. Ed.,* 2010**, 49,** 2988-3005.
4 L. Truebestein and T. A. Leonard, *Bioessays,* 2016**, 38,** 903-916.
5 J. Liu, Q. Zheng, Y. Deng, C.-S. Cheng, N. R. Kallenbach and M. Lu, *Proc. Natl. Acad. Sci. USA,* 2006**, 103,** 15457–15462.
6 M. O. Steinmetz, I. Jelesarov, W. M. Matousek, S. Honnappa, W. Jahnke, J. H. Missimer, S. Frank, A. T. Alexandrescu and R. A. Kammerer, *Proc. Natl. Acad. Sci. U S A,* 2007**, 104,** 7062–7067.
7 B. Apostolovic, M. Danial and H.-A. Klok, *Chem. Soc. Rev.,* 2010**, 39,** 3541-3575.
8 B. Ciani, S. Bjelić, S. Honnappa, H. Jawhari, R. Jaussi, A. Payapilly, T. Jowitt, M. O. Steinmetz and R. A. Kammerer, *Proc. Natl. Acad. Sci. U S A,* 2010**, 107,** 19850-19855.
9 S. Raman, G. Machaidze, A. Lustig, U. Aebi and P. Burkhard, *Nanomed. Nanotechnol. Biol. Med.,* 2006**, 2,** 95-102.
10 J. M. Fletcher, R. L. Harniman, F. R. H. Barnes, A. L. Boyle, A. Collins, J. Mantell, T. H. Sharp, M. Antognozzi, P. J. Booth, N. Linden, M. J. Miles, R. B. Sessions, P. Verkade and D. N. Woolfson, *Science,* 2013**, 340,** 595-599.
11 H. Gradišar, S. Božič, T. Doles, D. Vengust, I. Hafner-Bratkovič, A. Mertelj, B. Webb, A. Šali, S. Klavžar and R. Jerala, *Nat. Chem. Biol.,* 2013**, 9,** 362-366.
12 L. Jiang, D. Xu, K. E. Namitz, M. S. Cosgrove, R. Lund and H. Dong, *Small,* 2016**, 12,** 5126-5131.
13 S. Mondal and E. Gazit, *ChemNanoMat,* 2016**, 2,** 323-332.
14 A. Ljubetič, F. Lapenta, H. Gradišar, I. Drobnak, J. Aupič, Z. Strmšek, D. Lainšček, I. Hafner-Bratkovič, A. Majerle, N. Krivec, M. Benčina, T. Pisanski, T. C. Veličković, A. Round, J. M. Carazo, R. Melero and R. Jerala, *Nat. Biotechnol.,* 2017**, 35,** 1094-1101.
15 Y. Wu and J. H. Collier, *Wiley Interdiscip. Rev.: Nanomed. Nanobiotechnol.,* 2017**, 9,** 1-17.
16 J. M. Fletcher, K. A. Horner, G. J. Bartlett, G. G. Rhys, A. J. Wilson and D. N. Woolfson, *Chem. Sci.,* 2018**, 9,** 7656-7665.
17 L. Jiang, S. Yang, R. Lund and H. Dong, *Biomater. Sci.,* 2018**, 6,** 272-279.
18 S. Yagi, S. Akanuma and A. Yamagishi, *Biophys. Rev.,* 2018**, 10,** 411-420.
19 Y.-H. Watanabe, N. Yosuke, R. Suno and M. Yoshida, *Biochem. J,* 2009**, 421,** 71-77.
20 E. Lesne, E.-M. Krammer, E. Dupre, C. Locht, M. F. Lensink, R. Antoine and F. Jacob-Dubuissona, *MBio,* 2016**, 7,** e02089-02015.

21 H. Wang, M. H. Nada, Y. Tanaka, S. Sakuraba and C. T. Morita, *J. Immunol.,* 2019**, 203,** 607-626.
22 F. Thomas, A. L. Boyle, A. J. Burton and D. N. Woolfson, *J. Am. Chem. Soc.,* 2013**, 135,** 5161-5166.
23 Y. Tang, G. Ghirlanda, N. Vaidehi, J. Kua, D. T. Mainz, W. A. G. III, W. F. DeGrado and D. A. Tirrell, *Biochemistry,* 2001**, 40,** 2790-2796.
24 N. E. Zhou, C. M. Kay and R. S. Hodges, *Biochemistry,* 1993**, 32,** 3178-3187.
25 E. M. Goodman and P. S. Kim, *Biochemistry,* 1991**, 30,** 11615-11620.
26 L. B. Moran, J. P. Schneider, A. Kentsis, G. A. Reddy and T. R. Sosnick, *Proc. Natl. Acad. Sci. U S A,* 1999**, 96,** 10699-10704.
27 J. W. Blankenship, R. Balambika and P. E. Dawson, *Biochemistry,* 2002**, 41,** 15676-15684.
28 T. Wang, W. L. Lau, W. F. DeGrado and F. Gai, *Biophys. J.,* 2005**, 89,** 4180-4187.
29 P. Burkhard, S. Ivaninskii and A. Lustig, *J. Mol. Biol.,* 2002**, 318,** 901-910.
30 I. Drobnak, H. Gradišar, A. Ljubetič, E. Merljak and R. Jerala, *J. Am. Chem. Soc.,* 2017**, 139,** 8229-8236.
31 M. G. Wuo, A. B. Mahon and P. S. Arora, *J. Am. Chem. Soc.,* 2015**, 137,** 11618-11621.
32 M. G. Wuo, S. H. Hong, A. Singh and P. S. Arora, *J. Am. Chem. Soc.,* 2018**, 140,** 16284-16290.
33 I. Tunn, A. S. d. Léon, K. G. Blank and M. J. Harrington, *Nanoscale,* 2018**, 10,** 22725-22729.
34 K. S. Åkerfeldt, R. M. Kim, D. Camac, J. T. Groves, J. D. Lear and W. F. DeGrado, *J. Am. Chem. Soc.,* 1992**, 114,** 9656-9657.
35 M. Mutter, G. G. Tuchscherer, C. Miller, K.-H. Altmann, R. I. Carey, D. F. Wyss, A. M. Labhardt and J. E. Rivier, *J. Am. Chem. Soc.,* 1992**, 114,** 1463-1470.
36 J. P. Schneider and J. W. Kelly, *Chem. Rev.,* 1995**, 95,** 2169-2187.
37 A. K. Wong, M. P. Jacobsen, D. J. Winzor and D. P. Fairlie, *J. Am. Chem. Soc.,* 1998**, 120,** 3836-3841.
38 A. R. Mezo and J. C. Sherman, *J. Am. Chem. Soc.,* 1999**, 121,** 8983-8994.
39 J. Brask, J. M. Dideriksen, J. Nielsen and K. J. Jensen, *Org. Biomol. Chem.,* 2003**, 1,** 2247-2252.
40 H. Li and L.-X. Wang, *Org. Biomol. Chem.,* 2003**, 1,** 3507-3513.
41 J.-C. Horng, A. J. Hawk, Q. Zhao, E. S. Benedict, S. D. Burke and R. T. Raines, *Org. Lett.,* 2006**, 8,** 4735-4738.
42 A. S. Causton and J. C. Sherman, *J. Pept. Sci.,* 2002**, 8,** 275-282.
43 M. R. Ghadiri, C. Soares and C. Choi, *J. Am. Chem. Soc.,* 1992**, 114,** 825-831.
44 M. A. Case and G. L. McLendon, *Acc. Chem. Res.,* 2004**, 37,** 754-762.
45 H. Jang, A. Fafarman, J. M. Holub and K. Kirshenbaum, *Org. Lett.,* 2005**, 7,** 1951-1954.
46 J. M. Holub, H. Jang and K. Kirshenbaum, *Org. Biomol. Chem.,* 2006**, 4,** 1497-1502.
47 P. M. Levine, K. Imberg, M. J. Garabedian and K. Kirshenbaum, *J. Am. Chem. Soc.,* 2012**, 134,** 6912-6915.
48 P. M. Levine, E. Lee, Alex Greenfield, R. Bonneau, S. K. Logan, M. J. Garabedian and K. Kirshenbaum, *ACS Chem. Biol.,* 2012**, 7,** 1693-1701.
49 P. M. Levine, T. P. Carberry, J. M. Holub and K. Kirshenbaum, *MedChemComm,* 2013**, 4**.
50 R. N. Zuckermann, J. M. Kerr, S. B. H. Kent and W. H. Moos, *J. Am. Chem. Soc.,* 1992**, 114,** 10646-10647.
51 K. Kirshenbaum, A. E. Barron, R. A. Goldsmith, P. Armand, E. K. Bradley, K. T. V. Truong, K. A. Dill, F. E. Cohen and R. N. Zuckermann, *Proc. Natl. Acad. Sci. USA,* 1998**, 95,** 4303–4308.
52 P. Hosseinzadeh, G. Bhardwaj, V. K. Mulligan, M. D. Shortridge, T. W. Craven, F. Pardo-Avila, S. A. Rettie, D. E. Kim, D.-A. Silva, Y. M. Ibrahim, I. K. Webb, J. R. Cort, J. N. Adkins, G. Varani and D. Baker, *Science,* 2017**, 358,** 1461-1466.
53 T. A. Hill, N. E. Shepherd, F. Diness and D. P. Fairlie, *Angew. Chem. Int. Ed.,* 2014**, 53,** 13020-13041.
54 C. K. Wang, J. E. Swedberg, S. E. Northfield and D. J. Craik, *J. Phys. Chem. B,* 2015**, 119,** 15821-15830.
55 E. K. O'Shea, J. D. Klemm, P. S. Kim and T. Alber, *Science,* 1991**, 254,** 539-544.
56 F. Thomas, A. Niitsu, A. Oregioni, G. J. Bartlett and D. N. Woolfson, *Biochemistry,* 2017**, 56,** 6544-6554.
57 V. Hornak, R. Abel, A. Okur, B. Strockbine, A. Roitberg and C. Simmerling, *Proteins Struct. Funct. Bioinf.,* 2006**, 65,** 712-725.
58 H. Nguyen, J. Maier, H. Huang, V. Perrone and C. Simmerling, *J. Am. Chem. Soc.,* 2014**, 136,** 13959-13962.
59 H. Nguyen, D. R. Roe and C. Simmerling, *J. Chem. Theory Comput.,* 2013**, 9,** 2020-2034.
60 I. Izzo, G. Ianniello, C. D. Cola, B. Nardone, L. Erra, G. Vaughan, C. Tedesco and F. De Riccardis, *Org. Lett.,* 2013**, 15,** 598-601.
61 J. Wang, R. M. Wolf, J. W. Caldwell, P. A. Kollman and D. A. Case, *J. Comput. Chem.,* 2004**, 25,** 1157-1174.
62 S. B. Y. Shin, B. Yoo, L. J. Todaro and K. Kirshenbaum, *J. Am. Chem. Soc.,* 2007**, 129,** 3218-3225.
63 V. Hong, S. I. Presolski, C. Ma and M. G. Finn, *Angew. Chem. Int. Ed.,* 2009**, 48,** 9879-9883.
64 Y.-H. Chen, J. T. Yang and K. H. Chau, *Biochemistry,* 1974**, 13,** 3350-3359.
65 N. J. Greenfield, *Nat. Protoc.,* 2006**, 1,** 2527-2535.
66 N. E. Zhou, B.-Y. Zhu, C. M. Kay and R. S. Hodges, *Biopolymers,* 1992**, 32,** 419-426.
67 R. S. Kiss, P. M. M. Weers, V. Narayanaswami, J. Cohen, C. M. Kay and R. O. Ryan, *J. Biol. Chem.,* 2003**, 278,** 21952-21959.
68 R. O. Crooks, T. Rao and J. M. Mason, *J. Biol. Chem.,* 2011**, 286,** 29470-29479.
69 W. M. Park, M. Bedewy, K. K. Berggren and A. E. Keating, *Sci. Rep.,* 2017**, 7,** 10577.
70 W. Bai, C. J. Sargent, J.-M. Choi, R. V. Pappu and F. Zhang, *Nat. Commun.,* 2019**, 10,** 3317.